Geoderma 434 (2023) 116486

Contents lists available at ScienceDirect

Geoderma

journal homepage: www.elsevier.com/locate/geoderma

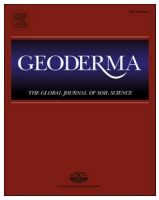

Kinetics of coupled sorption and abiotic oxidation of antimony(III) in soils

Tongliang Wu [a], Cun Liu [a], Peixin Cui [a], Hongjing Zhang [a], Sainan Hu [a], Peng Zhang [a], Qin Xue [a], Yaodong Wang [a], Chenglong Feng [b], Marcelo Eduardo Alves [c], Matthew K. Tighe [d], Yujun Wang [a,e,*]

[a] Key Laboratory of Soil Environment and Pollution Remediation, Institute of Soil Science, Chinese Academy of Sciences, Nanjing 210008, China
[b] State Key Laboratory of Soil Erosion and Dryland Farming on the Loess Plateau, Institute of Soil and Water Conservation, Northwest A&F University, Yangling 712100, Shaanxi, China
[c] Department of Exact Sciences 'Luiz de Queiroz' Agricultural College – ESALQ/USP, Piracicaba, SP 13418-900, Brazil
[d] School of Environmental and Rural Science, University of New England, Armidale NSW 2350, Australia
[e] University of Chinese Academy of Sciences, Beijing 100049, China

ARTICLE INFO

Handling Editor: Daniel Said-Pullicino

Keywords:
Kinetics
Kinetic model
Antimony
Soil
Adsorption and desorption
Oxidation

ABSTRACT

A quantitative evaluation of the dynamics of antimony (Sb) species transformation when Sb(III) enters the soil matrix would facilitate the understanding of the speciation and environmental fate of Sb in natural environments. Towards this end, the coupled sorption and abiotic oxidation kinetics of Sb(III) were examined across 12 soils with a 24 h timeframe. The soil-solution distribution coefficients (K_d) of Sb ranged between 214 and 5965 L kg^{-1}. Both apparent and mechanistic kinetic models were used to described the process. The apparent kinetic model indicated a two-rate oxidation and associated stabilization behavior of Sb in soils. The fast oxidation rate constants ranged from 0.147 to 0.763 h^{-1}, which were one to two orders of magnitudes higher than the slow rate constants (0.002–0.039 h^{-1}). Iron and Mn oxides were identified as the key soil components associated with adsorptive-oxidative sites (SOH) and oxidative sites (Mn-OH) of soils for Sb species, and these were subsequently integrated into the mechanistic kinetic model. This model included the adsorption–desorption of Sb(III) as well as the oxidation product, Sb(V) on the SOH, the oxidation of Sb(III) by SOH and Mn-OH, and the stabilization of both Sb(III) and Sb(V). The model produced a global fit for dissolved and adsorbed Sb species across the 12 soils. This study provides new information for predicting the dynamics of Sb in soils when multiple adsorption–desorption, oxidation and stabilization reactions are coupled in natural environments.

1. Introduction

Antimony (Sb) and its compounds have been received increasing attention due to their toxicity and possible carcinogenicity (He et al., 2018). Inorganic antimonite [Sb(III)] and antimonate [Sb(V)] are the most common forms of this metalloid present in the soil environment. Antimonite is initially released during mineral mining or smelting, and generally exhibits higher toxicity than Sb(V) (He et al., 2018; Zhang et al., 2022). This latter form is predominant in oxic soils, and existing as an oxyanion is relatively mobile in soils (Wilson et al., 2010). In most situations (away from areas of primary mineral formation), both Sb(III) and Sb(V) exist in a complex combination of dissolved and surface bound forms, with surface properties, pH and redox conditions governing speciation and mobility (Doherty et al., 2021).

Understanding immobilization and oxidation processes of Sb(III) in the soil matrix is essential for predicting the environmental fate and behavior of Sb. A major soil component known to influence Sb behavior are Fe (hydr)oxides, due to their abundance, high surface areas and reactivity (Guo et al., 2014; Scheinost et al., 2006). *In-situ* synchrotron based analysis has indicated the extensive correlation between Fe and Sb in soils, and bidentate mono- and binuclear inner-sphere surface complexation have been identified as the major Sb immobilization mechanisms on the surface of Fe oxides (Mitsunobu et al., 2010; Scheinost et al., 2006). Antimony may also be irreversibly immobilized by entering the lattice of the Fe oxides during phase transformation (Burton et al., 2020; Burton et al., 2019; Mitsunobu et al., 2013). In addition, Al/Mn oxides as well as soil organic matter can contribute to Sb immobilization due to their reactive surface functional groups (Besold et al., 2019; Ilgen and Trainor, 2011; Wang et al., 2021). Meanwhile, Mn(III/VI) oxides have been found to be the main oxidants

* Corresponding author.
E-mail address: yjwang@issas.ac.cn (Y. Wang).

https://doi.org/10.1016/j.geoderma.2023.116486
Received 24 May 2022; Received in revised form 29 March 2023; Accepted 18 April 2023
Available online 25 April 2023

for Sb(III) in soil (Belzile et al., 2001), and rapid oxidation of Sb(III) has been commonly observed by both amorphous and crystalline Mn oxides after inner-sphere complexation (Sun et al., 2019; Wang et al., 2021). Additionally, the oxidation of Sb(III) can be mediated by reactive oxygen species, including hydrogen peroxide and the superoxide radical anion, or semiquinone radicals (Leuz and Johnson, 2005; Wu et al., 2019a).

In the soil matrix, equilibrium experiments have mostly been adopted to evaluate the adsorption behaviors of Sb. Reported soil-solution distribution coefficients (K_d) of Sb vary widely, with values from 110 soil samples ranging from 1 to 2065 L kg^{-1} (Nakamaru et al., 2006; Tighe et al., 2005). The Langmuir and Freundlich equations have most often been applied to describe Sb soil sorption isotherms (Dousova et al., 2015; Fan et al., 2013; Martinez-Llado et al., 2011), while multilayer surface complexation modeling has been less commonly applied, but can give more details on surface binding modes. For example, Vithanage et al. (2013) applied 2-pK diffuse double layer model (DDLM) to Sb(V) sorption on red earth soils and found the sorption was dominated by Fe phases in forms of bidentate mono- and bi-nuclear complexation, which generally matched with X-ray absorption spectroscopy and density functional theory calculations that bidentate binuclear complexes between Sb(V) and goethite were thermodynamically favorable (Sun et al., 2023).

The equilibrium coefficients obtained from batch experiments may not sufficiently describe the dynamics of the geochemical processes of Sb, due to the physical and chemical non-equilibrium nature in soils. Kinetic experiments of Sb(III) retention in typical soils have been conducted and characteristic kinetic patterns with initially fast followed by slow rates were found (Li et al., 2018). Kinetic models incorporating both oxidation and adsorption processes have been used to describe and predict the multi-step processes of species and adsorption shifts of Sb over time in acidic red soil and calcareous soil (Cai et al., 2016; Zhang et al., 2014). It has been found that extensive oxidation of Sb(III) occurs quickly in soils and the oxidation kinetics largely determines the adsorption and transport of Sb (Xia et al., 2022). However, most previous studies have focused on the long-term kinetic behavior of Sb in soils, with time scales ranging from 10 to 55 days. Thus, the critical initial stages of the fast reactions between Sb(III) and soil components still require elucidation (Cai et al., 2016; Xia et al., 2022). In addition, to date kinetic rate coefficients of Sb behavior has only been obtained for a very limited range of soils, and Sb speciation changes on solid phases during this initial stage have not been clarified. Thus, further investigation on a wide range of soils to determine fundamental kinetic reaction processes of Sb is urgently needed.

In this study, the coupled dynamics of Sb(III) sorption and oxidation were investigated by exogenous addition of Sb(III) to 12 soils with a very wide range of properties across 24 h. The parameters generated from an apparent kinetic model were used to identify soil components strongly associated with Sb(III) behavior, which were subsequently incorporated into a mechanistic kinetic model. The objectives of this study were: (1) to quantitatively assess the contents of Sb(III) and Sb(V) in soil solutions and on solid phases simultaneously at different time intervals; (2) to identify key soil components influencing Sb K_d and apparent rate constants; (3) to establish a mechanistic kinetic model by integrating associated soil components, and to model oxidation and sorption dynamics of Sb(III) across a range of soils. Findings of this study could provide essential information to describe the environmental behaviors of Sb(III) across different soils and improve the understanding of the bioavailability and toxicity of Sb in aerobic soils.

2. Materials and methods

2.1. Chemical reagents

Antimony trioxide (Sb_2O_3, 99.999%), sodium perchlorate ($KClO_4$), ammonium oxalate [$(NH_4)_2C_2O_4$], ascorbic acid, sodium citrate dibasic ($C_6H_6O_7Na_2$), potassium hydroxide (KOH), hydrochloric acid (HCl), sodium fluoride (NaF), thiourea, potassium borohydride (KBH_4) and potassium phosphate monobasic (KH_2PO_4) were purchased from Aladdin Co. Ltd. (Shanghai, China). All chemicals were of at least analytical grade and the solutions were prepared with ultrapure deionized water (18.2 MΩ cm^{-1}). The stock solution of Sb(III) was prepared by dissolving Sb_2O_3 in 2.0 M HCl (Text S1).

2.2. Soil samples

Soil samples (0–20 cm) were collected from 12 provinces of China, covering six soil series with different physicochemical properties, including Inceptisols, Mollisols, Alfisols, Ultisol, Entisols, and Oxisol (Table S1). Soil pH was measured at soil:water = 1:2.5 ratio. Soil organic matter (OM) was measured by the dichromate method (Lu, 2000). Soil cation exchange capacity (CEC) was determined by the Ethylenediaminetetraacetic acid (EDTA)–ammonium acetate exchange method (Wang et al., 2020). Soil total phosphorus (P) was determined by alkaline digestion followed by molybdenum antimony blue colorimetry (Liu et al., 2013). The particle size distribution (sand%, silt% and clay%) was measured with the pipette method (Abdulaha-Al Baquy et al., 2018). The amorphous Fe, Mn and Al oxides (Fe-ox, Mn-ox and Al-ox) and the crystalline Fe, Mn and Al oxides (Fe-DCB, Mn-DCB and Al-DCB) were extracted by ammonium oxalate (pH 3.0) in the dark and dithionite-citrate-bicarbonate (DCB), respectively (Lu, 2000). Basic physicochemical properties of soils are shown in Table 1.

2.3. Kinetic experiments

Air-dried soils were ground to pass through a 250-μm sieve and sterilized by γ irradiation (50 k, Co source, BFT-IV, China) to exclude potentially microbially-mediated redox transformations (Chen et al., 2021). The batch kinetic experiments were started within 2 days after the sterilization. Briefly, 0.35 g soil was added to a 35 mL $KClO_4$ (10 mM) solution in 50-mL centrifuge tubes in duplicate. The suspensions were left to equilibrate on an end-over-end shaker for 24 h in the dark (200 rpm, 25 °C). The initial pH of soil suspensions (soil:$KClO_4$ solutions = 1:100) was measured in Table 1. Control experiment indicated no significant oxidation of Sb(III) was found in $KClO_4$ solution (Text S2, Fig. S1), which is supported by previous uses of $KClO_4$ in similar experiments (Fox et al., 2009; Gallard et al., 2009; Kong and He, 2016; Leuz et al., 2006; Pullin and Cabaniss, 2003).

An aliquot of Sb(III) from the stock solution was spiked into the suspensions to maintain a final concentration of 20 μM. The added Sb (III), existing as $Sb(OH)_3$, was soluble and below the solubility of Sb_2O_3 (Text S3, Fig. S2). The pH of suspensions was initially adjusted by 2 M HCl or 2 M NaOH and these pH values were not significantly changed (±0.2 pH unit) during reactions. The tubes were shaken continuously in the dark during the experiment periods. The concentration of Sb(III) (20 μM, 2.436 mg/L) was used as it is commonly found around mining and smelting sites, following initial release of Sb(III) from dissolution of Sb_2S_3 or Sb_2O_3 minerals (He et al., 2018) and this concentration has been previously used to explore the redox mechanisms of Sb(III) in environmental matrices (Kong and He, 2016; Kong et al., 2015).

Two suspension samples were simultaneously taken at 0.5, 1, 3.5, 7, 12 and 24 h. For Sb(III) and the oxidation product, Sb(V), in soil solution [sol-Sb(III) and sol-Sb(V)], a portion (1 mL) was filtered through 0.45-μm cellulose membranes and preserved in 0.5 M $C_6H_6O_7Na_2$ in the dark. The K_d values of Sb among the soils was calculated at 24 h. For extractable Sb species in suspensions [ex-Sb(III) and ex-Sb(V)], another portion (1 mL) was extracted by 5 mL 0.2 M $(NH_4)_2C_2O_4$/0.1 M ascorbic acid/0.2 M KH_2PO_4 (pH 3.25) in a water bath at 96 °C for 30 min with intermittent stirring. Therefore, our initial sampling point was set at 0.5 h due to the limitation of the chemical extraction procedure in which the water bath step costed 0.5 h. This approach was modified from (Leuz, 2006), and is often applied to estimate the fraction associated with

Table 1
Basic physicochemical properties of investigated soils.

No.	Soil	Classification	Soil pH	Suspension pH	OM g kg^{-1}	Sand (%)	Silt (%)	Clay (%)	CEC cmol kg^{-1}	P g kg^{-1}	Fe-ox Fe, g kg^{-1}	Mn-ox Mn, g kg^{-1}	Al-ox Al, g kg^{-1}	Fe-DCB Fe_2O_3, g kg^{-1}	Mn-DCB MnO, g kg^{-1}	Al-DCB Al_2O_3, g kg^{-1}
1	Hebei	Inceptisol	8.21	7.79	7.90	26.83	58.83	14.35	9.50	0.72	1.25	0.33	0.73	5.97	0.18	0.56
2	Shaanxi	Mollisol	8.25	9.00	14.60	4.85	80.03	15.12	10.54	0.90	0.52	0.35	0.70	6.58	0.37	0.52
3	Anhui	Alfisol	5.29	5.57	21.88	19.70	50.66	29.64	14.41	0.70	1.98	0.44	1.30	23.93	0.43	2.86
4	Yunnan	Alfisol	6.93	6.31	26.52	39.06	36.20	24.74	16.13	1.25	5.99	0.19	0.78	15.18	0.09	1.03
5	Guangdong	Ultisol	4.91	5.22	46.10	14.98	45.08	39.94	18.00	0.57	7.87	0.12	1.03	20.52	0.03	1.37
6	Chongqing	Entisol	6.40	6.39	17.00	33.24	48.82	17.94	24.25	0.65	2.95	0.27	0.57	9.09	0.17	0.40
7	Sichuan	Alfisol	8.09	8.03	11.60	26.18	58.25	15.58	19.89	0.63	1.37	0.48	0.67	7.05	0.52	0.57
8	Jiangsu	Alfisol	7.44	6.93	22.56	9.08	69.16	21.76	18.43	0.72	5.06	0.22	0.87	13.06	0.23	1.05
9	Zhejiang	Alfisol	6.82	6.19	33.43	7.96	65.80	26.24	20.42	0.55	6.11	0.21	0.89	8.07	0.13	0.69
10	Hubei	Ultisol	5.61	5.07	29.48	9.86	65.70	24.44	9.81	0.39	3.95	0.02	0.87	11.28	0.03	1.23
11	Jiangxi	Ultisol	4.91	4.80	10.11	19.72	41.72	38.56	12.07	0.62	3.45	0.14	2.12	23.04	0.16	3.77
12	Hainan	Oxisol	6.07	6.12	14.37	26.72	36.84	36.44	10.58	0.68	1.78	0.55	1.33	79.08	1.28	4.97

crystalline Fe oxides (Shuman, 1982). Phosphate was added to compete with Sb for the binding sites on the remaining phases (Biver et al., 2011; Xia et al., 2022). As with $KClO_4$, unintended species transformations from the oxalate extract were tested and found to be negligible in a control experiment (Text S4, Fig. S3). The suspensions were filtered through 0.45-μm cellulose membranes and preserved in the dark. The non-extractable Sb was defined as stabilized Sb (stab-Sb), which was calculated from the difference between the total added Sb and the Sb species in solution. The amount of adsorbed Sb species [SOSb(III) and SOSb(V)] was determined as the difference between the extractable Sb and the Sb in solution. The concentration of the Sb species was determined by hydride generation atomic fluorescence spectrometry (HG-AFS, BAF-2000, Beijing Baode Instrumental Company, Beijing, China) as described in detail in our previous study (Wu et al., 2019b).

2.4. Kinetic modeling

2.4.1. Apparent kinetic model

The dynamics of extractable and non-extractable Sb in soil suspensions was described by an apparent rate law. Considering the drastic change of ex-Sb(III), ex-Sb(V) and stab-Sb in the first hour, model equations were solved piecewise (≤1h and > 1 h), and the following mass balance expression was used:

$$[Sb]_0 = [\text{ex-Sb(III)}] + [\text{ex-Sb(V)}] + [\text{stab-Sb}] \quad \text{(Eq. 1)}$$

where $[Sb]_0$ is initial Sb(III) added to suspensions, [ex-Sb(III)] and [ex-Sb(V)] are extractable Sb(III) and Sb(V), respectively, and [stab-Sb] is non-extractable Sb.

The expressions for extractable Sb(III) and Sb(V) are:

$$[\text{ex-Sb(III)}] = [\text{SOSb(III)}] + [\text{sol-Sb(III)}] \quad \text{(Eq. 2)}$$

and

$$[\text{ex-Sb(V)}] = [\text{SOSb(V)}] + [\text{sol-Sb(V)}] \quad \text{(Eq. 3)}$$

The conceptual model for the transformation of Sb in soil suspensions can be described as followed (Manning and Suarez, 2000):

$$[\text{ex} - \text{Sb(III)}] \xrightarrow{k_1} [\text{ex} - \text{Sb(V)}] \xrightarrow{k_2} [\text{stab} - \text{Sb}] \quad \text{(Eq. 4)}$$

$$\frac{d[\text{ex-Sb(III)}]}{dt} = -k_1[\text{ex-Sb(III)}] \quad \text{(Eq. 5)}$$

$$\frac{d[\text{ex-Sb(V)}]}{dt} = k_1[\text{ex-Sb(III)}] - k_2[\text{ex-Sb(V)}] \quad \text{(Eq. 6)}$$

$$[\text{stab-Sb}] = [Sb]_0 - [\text{ex-Sb(III)}] - [\text{ex-Sb(V)}] \quad \text{(Eq. 7)}$$

where k_{1fast} and k_{1slow} were defined as apparent fast and slow oxidation rate constants, respectively; k_{2fast} and k_{2slow} were defined as apparent fast and slow stabilization rate constants, respectively. The model equations were solved piecewise (≤1h and > 1 h).

2.4.2. Mechanistic kinetic model

The kinetic data of the coupled Sb redox and immobilization reactions in 12 soils were globally modeled by Kintecus V6.51 (Ianni, 2018). The concentrations of sol-Sb(III), sol-Sb(V), SOSb(III), SOSb(V) and stab-Sb at different time intervals were modeled and the reaction networks in Table 2 were used for kinetic modeling. Detailed calculations for model input are explained in Text S5. Briefly, the reactive sites on the key soil components, i.e. Fe oxides (Fe-ox and Fe-DCB) and Mn oxides (Mn-ox and Mn-DCB) were chosen to represent the adsorptive-oxidative sites (SOH) and oxidative sites (Mn-OH) of soil, respectively. The ratio of the fast oxidative sites (Mn_f-OH) and slow oxidative sites (Mn_s-OH) was 1/3 based on Amirbahman et al. (2006). This type of simplification and assumption was undertaken to minimize the reactants in the kinetic model and focus on known dominant processes in the soil, and has been used previously to increase the general understanding of thermodynamic and kinetic processes of As(III)/As(V) and phosphate binding in soils (Amirbahman et al., 2006; Cui and Weng, 2013).

Reactions 1–4 described the adsorption and desorption reactions of Sb(III) and Sb(V) with the surface reaction sites on Fe oxides. Reactions 5–7 indicated the oxidation of Sb(III) on the Fe oxides and fast/slow oxidative sites on the Mn oxides, respectively. Reactions 8–9 and 10–11 described the stabilization processes of Sb(III) and Sb(V), respectively. Sensitivity analysis was performed by comparing the normalized sensitivity cofficients (NSCs) to evaluated the relative importance of each reaction for dynamics of Sb(III) and Sb(V) in soil solution as well as adsorbed Sb(III) and Sb(V). The positive and negative NSCs represent sources and sinks of reactants in the model (Ianni, 2018).

Table 2
Reaction network of the mechanistic kinetic model and rate constants between Sb and soil components.

No.	Reactions	Reaction constants (k)
1	SOH + Sb(III) → SOSb(III)	2.83 $M^{-1}s^{-1}$ [a]
2	SOSb(III) → SOH + Sb(III)	3.95×10^{-5} s^{-1} [b]
3	SOH + Sb(V) → SOSb(V)	1.41×10^{-1} $M^{-1}s^{-1}$ [a]
4	SOSb(V) → SOH + Sb(V)	1.32×10^{-5} s^{-1} [b]
5	SOSb(III) → SOSb(V)	3.89×10^{-6} s^{-1} [b]
6	Mn_f-OH + Sb(III) → Sb(V) + Mn(II)	6.00×10^{1} $M^{-1}s^{-1}$ [a]
7	Mn_s-OH + Sb(III) → Sb(V) + Mn(II)	3.63 $M^{-1}s^{-1}$ [a]
8	Sb(III) → stab-Sb	7.28×10^{-5} s^{-1} [a]
9	stab-Sb → Sb(III)	1.10×10^{-5} s^{-1} [a]
10	Sb(V) → stab-Sb	5.05×10^{-6} s^{-1} [c]
11	stab-Sb → Sb(V)	1.17×10^{-6} s^{-1} [c]

Note: [a]: fitted in this study; [b]: Cai et al., 2016; [c]: Xia et al., 2022.

2.5. Statistical analysis

Spearman correlations (due to non-normality of data) were carried out to determine the association between soil properties and thermodynamic and kinetic parameters (i.e. K_d, k_{1fast}, k_{1slow} and k_{2fast}) of Sb. Stepwise regression was used to further explore the effect of the above soil properties on both parameters with the criteria that the probability for variables entering $F \leq 0.05$, and the probability for variables removing $F \geq 0.1$. The r and R^2 in this study represent Spearman's rank correlation coefficient and adjusted coefficient of determination of the prediction models, respectively. Spearman correlations were performed by "cor" from package "stats" in R (https://www.r-project.org/), and the package "heatmap3" enabled drawing heat-maps. Stepwise multiple linear regressions were performed SPSS software package version 21.0.

3. Result and discussion

3.1. Soil characteristics

As shown in Table 1, the test soils exhibited contrasting properties with pH values ranging from 4.91 to 8.25 and OM content ranging from 7.90 to 46.10 g kg^{-1}. Soils from Anhui, Guangdong, Jiangxi and Hainan were relatively high in Fe-DCB contents (20.52–79.08 g kg^{-1}) and the contents from the other soils were relatively low (5.97–15.18 g kg^{-1}). The Mn-DCB contents in the soils from Shaanxi, Anhui, Sichuan and Hainan were varied from 0.37 to 1.28 g kg^{-1}, which was higher than the rest of the soils (0.03–0.23 g kg^{-1}). The Hainan soil had the highest Fe-DCB and Mn-DCB contents (79.08 and 1.28 g kg^{-1}, respectively) among all the test soils which could potentially affect the adsorption and oxidation of Sb(III) in soils.

3.2. Dynamics of Sb species in soil solution during solid–liquid partitioning

The sol-Sb(III) and sol-Sb(V) generally underwent a fast reaction with bulk soil followed by a slow one (Fig. 1). The sol-Sb(III) concentration sharply decreased by consistently>73.6% and there was a concurrent rapid increase in the sol-Sb(V) concentration for the first hour. These trends slowed afterwards. The K_d values ranged between 214 and 5965 L kg^{-1}, and agree with previously determined values (1–2065 L kg^{-1}) (Nakamaru et al., 2006), except for the extremely high value (5965 L kg^{-1}) of the Hainan soil, which can be explained by its highest content of Fe/Al oxides among all test soils. The K_d values were positively correlated with Al-ox, Al-DCB, Clay, Fe-ox and Fe-DCB, and grouped together with each other (Fig. 2).

Iron oxides were further identified as the major soil components associated with Sb sorption, as compared with other measured soil properties. The stepwise linear regression of K_d with soil properties resulted in the following equation:

$$\log K_d = 0.995 \log \text{Fe-DCB} + 1.664 \ (R^2 = 0.579, F = 16.156, P < 0.05) \quad \text{(Eq. 8)}$$

Considering their high abundance and known role in binding, the crystalline Fe oxides e.g., goethite, hematite and lepidocrocite, could effectively promote Sb immobilization (Sun et al., 2023; Guo et al., 2014; Scheinost et al., 2006), with the adsorbed-Sb associated with the crystalline Fe oxides representing the majority of the Sb(III) and Sb(V) immobilized by the soil matrix (Leuz, 2006). The electro-neutral Sb(III) could be effectively immobilized by the crystalline Fe oxides over a wide range of pH by forming inner-sphere complexes (Leuz et al., 2006).

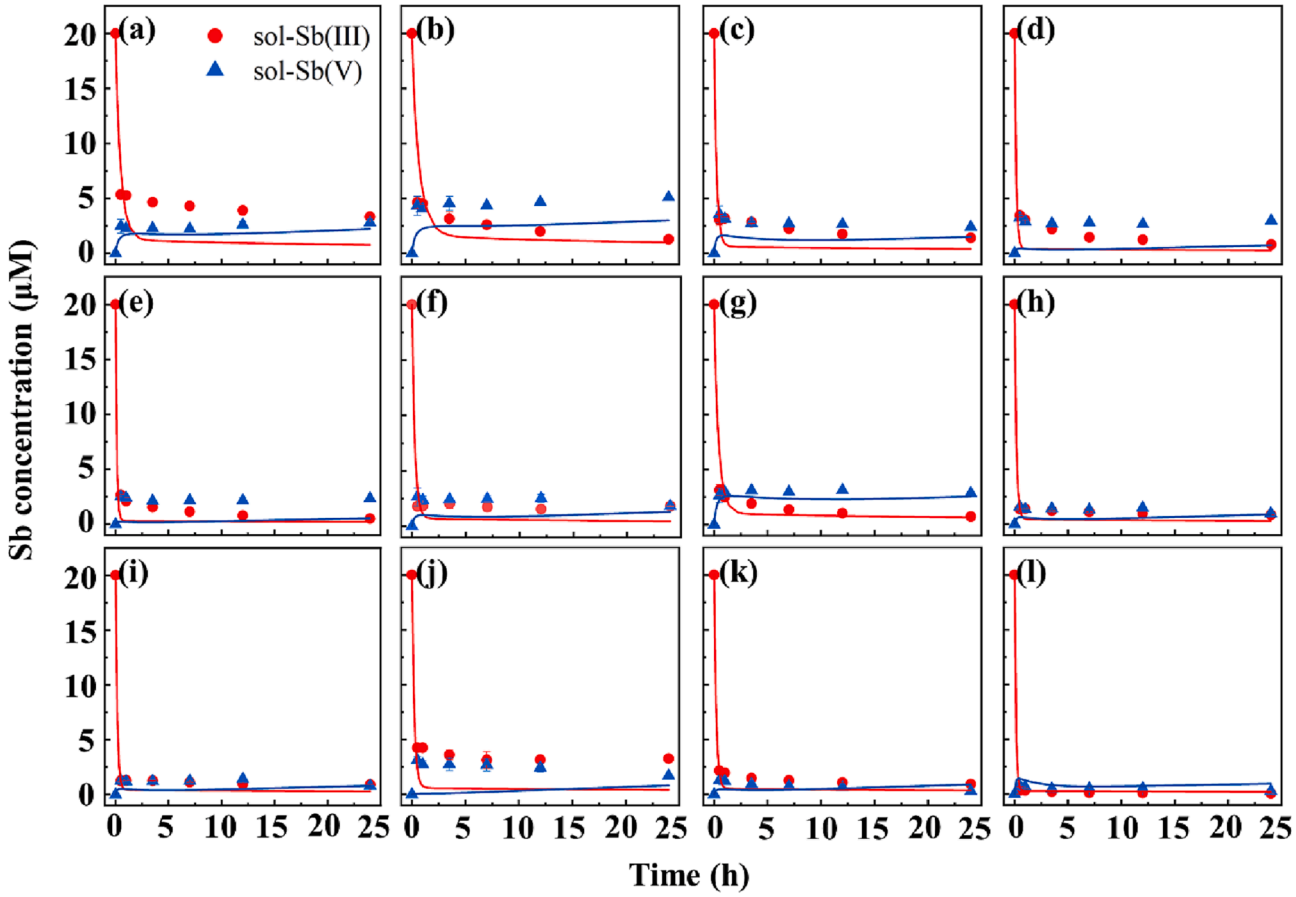

Fig. 1. Dynamics of Sb(III) and Sb(V) in soil solution from (a) Hebei, (b) Shaanxi, (c) Anhui, (d) Yunnan, (e) Guangdong, (f) Chongqing, (g) Sichuan, (h) Jiangsu, (i) Zhejiang, (j) Hubei, (k) Jiangxi and (l) Hainan soils. All lines are model fits to the experimental data from the mechanistic kinetic model.

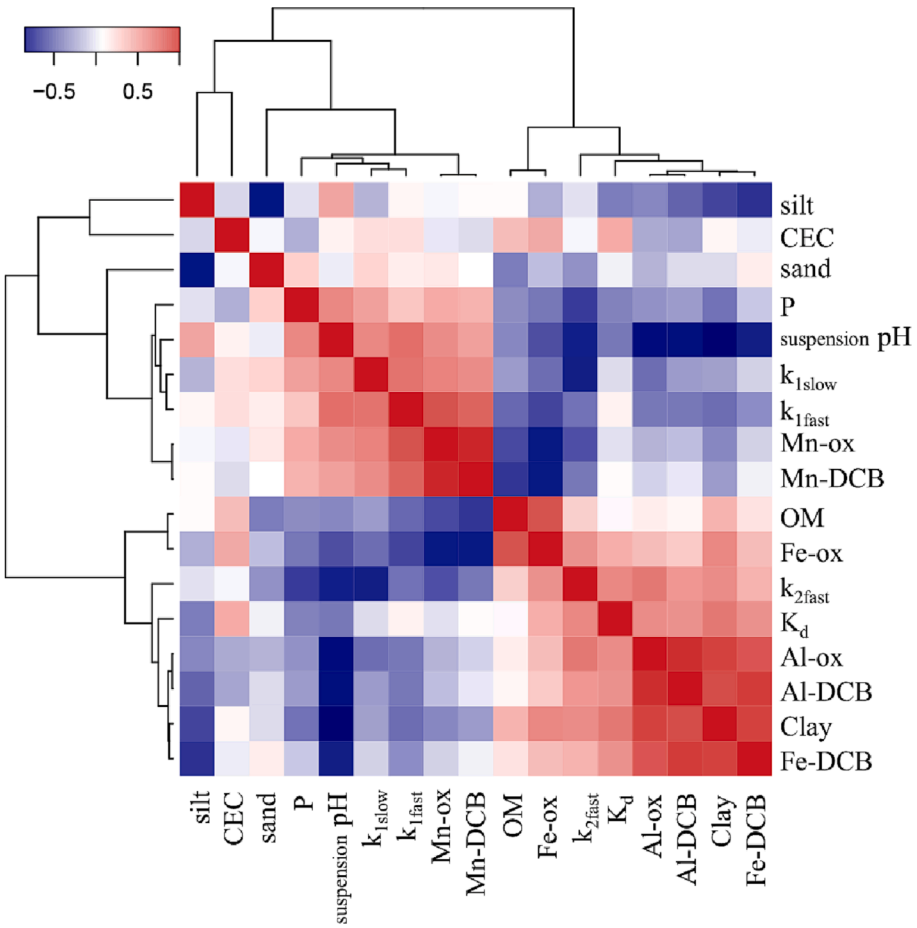

Fig. 2. Heat-maps of Spearman correlations of soil properties and soil-solution distribution coefficients (K_d), fast and slow Sb(III) oxidation (k_{1fast} and k_{1slow}) and stabilization rate constants (k_{2fast}).

Antimonite is also readily oxidized by soil minerals, including Mn oxides and Fe oxides, as discussed later. The generated Sb(V), existing as an oxyanion, predominates in oxic soil environments, and is most likely also be effectively immobilized on the crystalline Fe oxides due to its high pH_{PZC} (pH 7.3–7.8) by forming edge-sharing and bidentate corner-sharing complexes (Burton et al., 2020). In addition, the amorphous Fe oxides (e.g., ferrihydrite), usually contain a large specific area and are also effective scavengers for Sb in soils via the formation of inner-sphere complexes (Burton et al., 2019; Hockmann et al., 2021), though they were not identified by the stepwise regression analysis.

Thus, for the purpose of the modeling, it is reasonable to assume Sb immobilization was strongly associated with the contents of both crystalline and amorphous soil Fe oxides.

3.3. Describing extractable and non-extractable Sb with an apparent kinetic model

The extraction of Sb(III) and Sb(V) (as described in section 2.3) was used to assess the fraction of Sb(III) or Sb(V) in whole soil suspensions without changing their oxidation states (Leuz, 2006). The extraction efficiency of Sb in the 12 soils after 24 h were in the range of 70.2–91.1% (Table 3), similar to previous work and indicating the relative high efficiency of the extraction method (Leuz, 2006).

This model well described the dynamics of ex-Sb(III), ex-Sb(V) and stab-Sb during the experiments (Fig. 3). The oxidation rate constants (k_{1fast} and k_{1slow}) and the stabilization rate constants (k_{2fast} and k_{2slow}) are shown in Table 3. k_{1fast} ranged from 0.147 to 0.763 h^{-1}, and were one to two orders of magnitude higher than k_{1slow} (0.002–0.039 h^{-1}). Mn oxides (Mn-DCB and Mn-ox) were identified as key soil components for Sb

Table 3
Soil-solution distribution coefficients, extraction efficiency, oxidation and stabilization rate constants of Sb in the 12 soils.

No.	Soil	K_d (L kg^{-1})	Extraction efficiency (%)	Oxidation rate constants (h^{-1})		Stabilization rate constants (h^{-1})	
				k_{1fast}	k_{1slow}	k_{2fast}	k_{2slow}
1	Hebei	226	90.7	0.277	0.009	0.849	0.000
2	Shaanxi	214	85.4	0.424	0.028	0.783	0.007
3	Anhui	425	90.1	0.231	0.011	0.855	0.000
4	Yunnan	430	89.5	0.246	0.016	0.827	0.000
5	Guangdong	599	86.9	0.202	0.013	1.286	0.009
6	Chongqing	447	87.7	0.297	0.016	1.129	0.012
7	Sichuan	459	86.1	0.453	0.039	0.751	0.003
8	Jiangsu	994	86.8	0.266	0.012	1.790	0.000
9	Zhejiang	1069	80.7	0.286	0.006	4.163	0.000
10	Hubei	303	91.1	0.147	0.002	3.479	0.000
11	Jiangxi	1518	83.7	0.206	0.007	6.776	0.000
12	Hainan	5965	70.2	0.763	0.019	1.681	0.000

(III) oxidation (Fig. 2), as k_{1fast} was significantly positively correlated with both Mn-DCB and Mn-ox ($r = 0.739$ and 0.818, respectively, $P < 0.05$), meanwhile k_{1slow} was positively correlated with Mn-ox ($r = 0.627$, $P < 0.05$). The importance of these Mn phases in relation to the rate constants of Sb(III) oxidation are demonstrated by the stepwise linear regressions:

$$\log k_{1fast} = 0.334 \log \text{Mn-DCB} - 0.294 \ (R^2 = 0.686, F = 25.053, P < 0.05) \quad \text{(Eq. 9)}$$

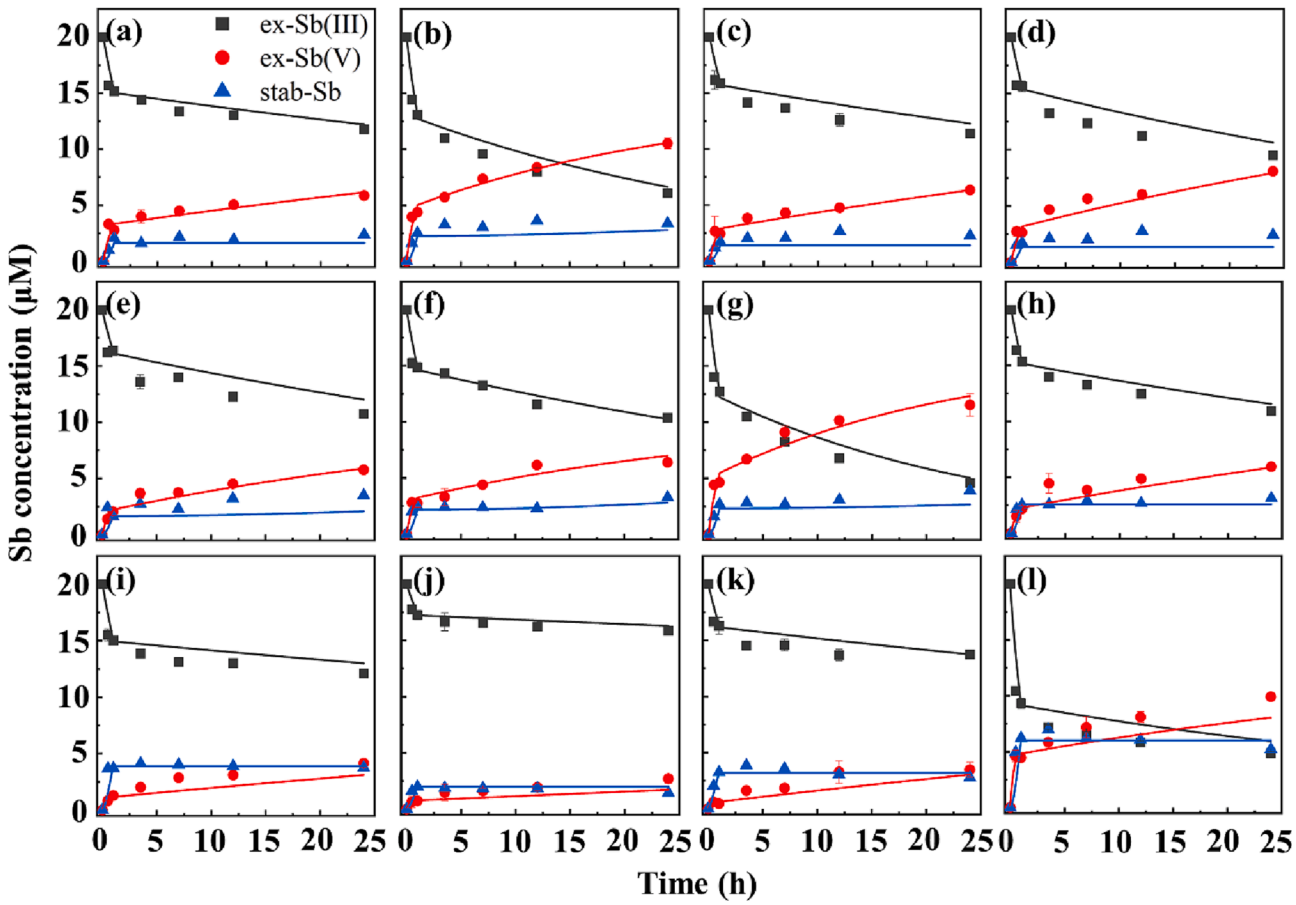

Fig. 3. Dynamics of extractible Sb(III), Sb(V) and stabilized Sb in soil suspensions from (a) Hebei, (b) Shaanxi, (c) Anhui, (d) Yunnan, (e) Guangdong, (f) Chongqing, (g) Sichuan, (h) Jiangsu, (i) Zhejiang, (j) Hubei, (k) Jiangxi and (l) Hainan soils. All lines are model fits to the experimental data from the apparent kinetic model. $\log k_{1slow} = 0.701 \log$ Mn-ox $- 1.465$ ($R^2 = 0.617$, $F = 18.694$, $P < 0.05$)(Eq. 10)

Similar two-rate behaviors have been observed in Sb(III) and As(III) oxidation kinetics in soil and/or aquifer materials (Amirbahman et al., 2006; Cai et al., 2016; Manning and Suarez, 2000). The oxidation rate constants in this study agreed with the apparent oxidation rate constants of As(III) in soils (0.0496–0.2905 h^{-1} for the fast oxidation process, 0.0082–0.0412 h^{-1} for the slow oxidation process) (Manning and Suarez, 2000). The *ex-situ* analysis in this study may not adequately characterize some rapid adsorption–desorption and redox reactions between Sb(III) and certain soil components that possibly occur at hotspots under microscopic scale. However, our time-averaging results (k_{1fast} and k_{1slow}) can still be considered representative of the macroscopic scale since they are consistent with the oxidation rate constants obtained from batch reactions between MnO_2 and Sb(III) (0.645–1.742 h^{-1}) (Zhang et al., 2020) and As(III) (0.37–5.4 h^{-1}) (Power et al., 2005; Villalobos et al., 2014) with a shorter first sampling point (2 min). Furthermore, the values are broadly consistent the oxidation rate constants of As(III) by MnO_2 obtained by quick-scanning X-ray absorption spectroscopy which ranged from 1.764 to 16.92 h^{-1}, and were obtained with sub-second time-resolution (Ginder-Vogel et al., 2009).

Mn oxides, exhibiting high oxidizing capacity and large specific surface area, are known to control Sb(III) oxidation in natural soils and sediments (Belzile et al., 2001). Antimonite has been found to be effectively oxidized by the reactive Mn(IV) sites on the edge of Mn oxides with different degrees of crystallinity, and the oxidation product Sb (V) subsequently released to the soil solution (Shi et al., 2018; Wang et al., 2021). Considering the complex structure of soils, diffusion-limited transport within soil aggregates could complicate the oxidation reaction rates between Sb(III) and Mn oxides (Ying et al., 2012). It is possible that the amorphous Mn oxides contained a higher number of internal oxidative sites compared with the crystalline phases, so that once the fast oxidation sites were depleted, Sb(III) needs to overcome the diffusion resistance to reach the internal sites to proceed with further oxidation. This could possibly explain why Mn oxides of varying levels of crystallinity were related to fast and slow oxidation rates at different stages of the examined reactions. Iron oxides could also catalyze Sb(III) oxidation in addition to having a high adsorption capacity. Previous work has also indicated that the formation of an inner-sphere complex between Sb(III) and goethite could increase the electron density of the Sb atom, facilitating its electron transfer to O_2 (Leuz et al., 2006), and similar results have been found with hydrous ferric oxide (Guo et al., 2014).

Based on the model assumptions, ex-Sb(V) could be transformed to stab-Sb. The intraparticle diffusion of Sb(V) to internal surface sorption sites in soil could also contribute to irreversible binding, which has been observed during Sb and As ageing in soil (Rahman et al., 2019; Verbeeck et al., 2021).

3.4. Incorporating soil components into the mechanistic rate law

To globally describe the multi-step reactions of Sb(III) in the different soils, a mechanistic rate law was developed with Kintecus V6.51 (Ianni, 2018). This model described the Sb(III) and Sb(V) in soil solution (Fig. 1), and also successfully modeled the adsorbed Sb(III) and Sb(V) [SOSb(III) and SOSb(V), respectively], as well as stab-Sb (Fig. 4). SOH was assumed to account for all the reversible adsorptive sites for Sb(III) and Sb(V), as described in Reactions 1–4 (Table 2). This was supported by sensitivity analysis that indicated the adsorption of Sb(III) (Reaction 1) and Sb(V) (Reaction 3) were the major sinks of Sb(III) (Fig. S4) and Sb

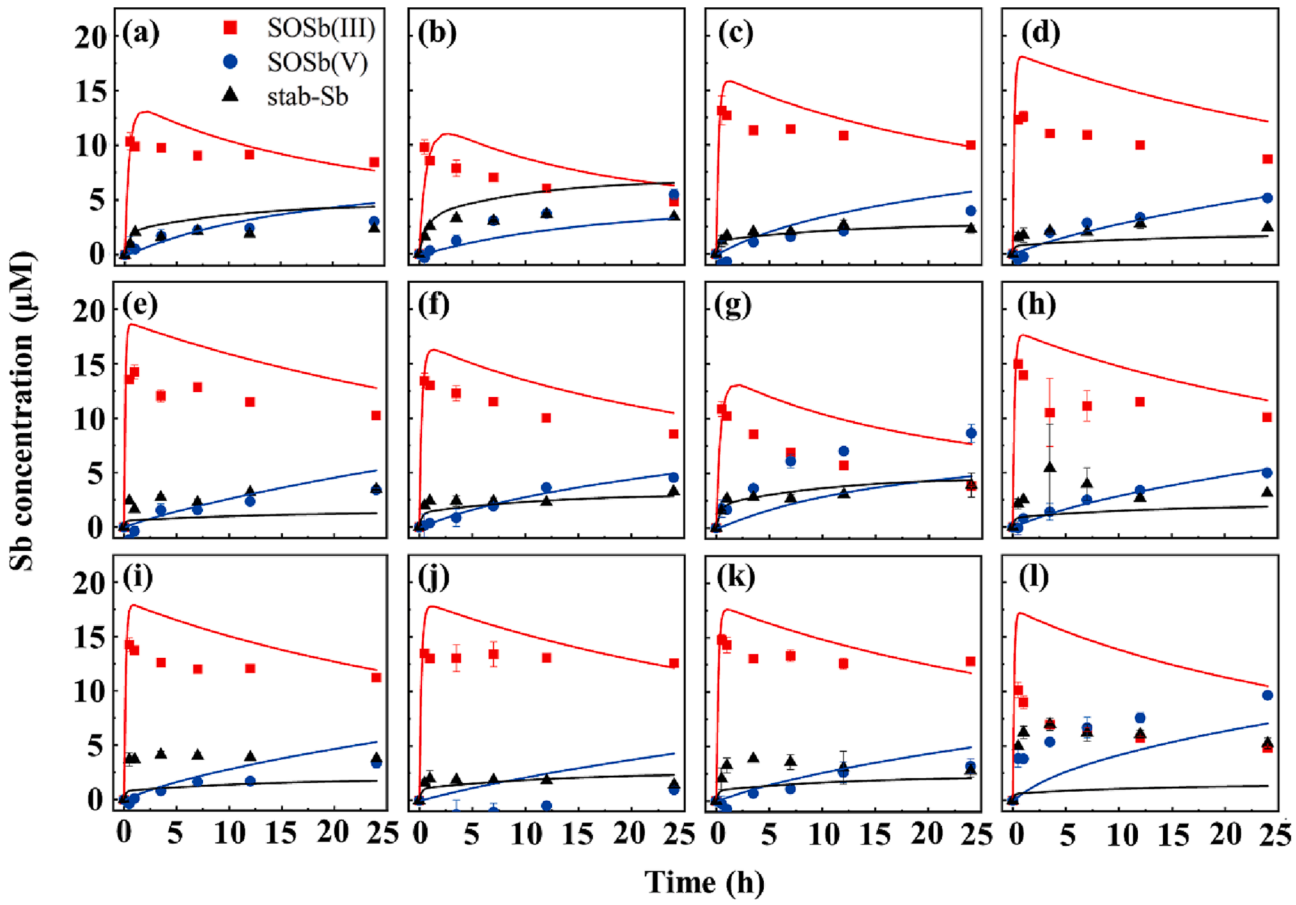

Fig. 4. Dynamics of adsorbed Sb(III) and Sb(V) and stabilized Sb in soil suspensions from (a) Hebei, (b) Shaanxi, (c) Anhui, (d) Yunnan, (e) Guangdong, (f) Chongqing, (g) Sichuan, (h) Jiangsu, (i) Zhejiang, (j) Hubei, (k) Jiangxi and (l) Hainan soils. All lines are model fits to the experimental data from the mechanistic kinetic model.

(V) (Fig. S5) in the model. Additionally, the higher adsorption rate constant for Sb(III) on SOH (2.83 $M^{-1}s^{-1}$) compared with Sb(V) (1.41 × 10^{-1} $M^{-1}s^{-1}$) agreed with the greater affinity of Sb(III) for Fe oxides compared with Sb(V) (Sun et al., 2023; Leuz et al., 2006). The desorption rates for Reactions 2 and 4, as well as the catalytic oxidation rate for Reaction 5, were fitted and constrained with published values (Cai et al., 2016). The adsorbed Sb(III) [SOSb(III)] could be catalytically oxidized to Sb(V) on the surface of Fe oxides (Reaction 5, Table 2) (Leuz et al., 2006), which positively contributed to the formation of SOSb(V) (Fig. S6–7).

The reactions between Sb(III) and Mn oxides have been investigated extensively (Shi et al., 2018; Sun et al., 2018). Generally, the process involved is Sb(III) adsorption on the oxidative sites and fast electron transfer after the formation of an inner-sphere complex, followed by the surface-bound Sb(V) being released to the solution. To keep a simple set of the reaction networks and reduce the fitting parameters, fast and slow reactions between Sb(III) and Mn oxides were described in Reactions 6–7, respectively (Table 2), and Mn(IV) phases were assumed to be the primary oxidative sites. The fitted rate constant for Sb(III) oxidation on Mn_f-OH (60.0 $M^{-1}s^{-1}$) was much higher than that on Mn_s-OH (3.63 $M^{-1}s^{-1}$). In addition, the contribution of Reaction 6 to Sb(V) generation decreased, which could be explained by the fast consumption of Mn_f-OH during the experiments (Fig. S5).

The stabilization process of Sb(III) and Sb(V) in soil was described by Reactions 8–11. Because the stab-Sb was defined as the non-extractable Sb fraction by the one-step extraction method used in this study, other immobilization mechanisms may be involved in this stabilization process, including the intraparticle diffusion of Sb(III) and Sb(V) and their potential association with clay minerals or soil organic matter (Besold et al., 2019; Dou et al., 2015; Ilgen and Trainor, 2011). The higher rate constant of Reaction 8 (7.28 × 10^{-5} s^{-1}) compared with Reaction 10 (5.05 × 10^{-6} s^{-1}) could be explained by the higher reactivity of Sb(III) in forming inner-sphere complexes with O/S-bearing surface groups on these soil components (Besold et al., 2019).

The differences between experimental data and modeling results (Fig. 4) indicated some important processes or phases were omitted from consideration, especially when describing the dynamics of Sb(III) adsorption on the soil with a high content of Fe-DCB, e.g., Hainan soil (Fig. 4l). The relatively large variation may arise from the inaccurate estimation of reactive adsorption sites on Fe oxides. Due to the complexity of soils, the reactive adsorption sites could be at least partially covered by mineral assemblages and soil particle aggregation, which may vary with soils and limit the fast and direct contact with Sb (III) (Davis et al., 1998; Tombacz et al., 2004). Furthermore, Fe oxides are major sinks for soil organic matter, and the formation of mineral-organic associations could also compete for surface hydroxyl groups, and decrease the adsorption capacity for metal(loid)s in soils, including Sb (Kleber et al., 2015; Lehmann and Kleber, 2015; Wu et al., 2019b).

4. Conclusion

The dynamics of Sb species in soil solutions and solids was assessed across 12 soils comprising a very wide range of properties known to influence Sb binding. The K_ds ranged between 214 and 5965 L kg^{-1} after 24 h. The apparent kinetic model indicated two-rate oxidation and stabilization behaviors of Sb in the soils. Iron and Mn oxides were identified as the key soil components associated with adsorptive-oxidative and oxidative sites respectively. The mechanistic kinetic

model established described both the Sb(III) and Sb(V) in soil solution, and the adsorbed Sb(III) and Sb(V). However, an accurate estimation of the reactive sites on Fe/Mn oxides in different soils is imperative for further investigations.

CRediT authorship contribution statement

Tongliang Wu: Investigation, Writing – original draft, Writing – review & editing, Data curation, Funding acquisition. **Cun Liu:** Conceptualization, Methodology. **Peixin Cui:** Conceptualization, Methodology. **Hongjing Zhang:** Investigation. **Sainan Hu:** Investigation. **Peng Zhang:** Investigation. **Qin Xue:** . **Yaodong Wang:** Investigation. **Chenglong Feng:** Investigation. **Marcelo Eduardo Alves:** Conceptualization, Writing – review & editing. **Matthew K. Tighe:** Conceptualization, Writing – review & editing. **Yujun Wang:** Conceptualization, Methodology, Writing – review & editing, Funding acquisition, Supervision.

Declaration of Competing Interest

The authors declare that they have no known competing financial interests or personal relationships that could have appeared to influence the work reported in this paper.

Data availability

Data will be made available on request.

Acknowledgements

This work was supported by the National Key Research and Development Program of China (2021YFC1809100), and the National Natural Science Foundation of China (42107041), and the Natural Science Foundation of Jiangsu Province, China (BK20210997), and China Postdoctoral Science Foundation (2020 M681754).

Appendix A. Supplementary data

Supplementary data to this article can be found online at https://doi.org/10.1016/j.geoderma.2023.116486.

References

Abdulaha-Al Baquy, M., Li, J.Y., Jiang, J., Mehmood, K., Shi, R.Y., Xu, R.K., 2018. Critical pH and exchangeable Al of four acidic soils derived from different parent materials for maize crops. J. Soils Sed. 18 (4), 1490–1499.

Amirbahman, A., Kent, D.B., Curtis, G.P., Davis, J.A., 2006. Kinetics of sorption and abiotic oxidation of arsenic(III) by aquifer materials. Geochim. Cosmochim. Acta 70 (3), 533–547.

Belzile, N., Chen, Y.W., Wang, Z.J., 2001. Oxidation of antimony(III) by amorphous iron and manganese oxyhydroxides. Chem. Geol. 174 (4), 379–387.

Besold, J., Kumar, N., Scheinost, A.C., Lezama Pacheco, J., Fendorf, S., Planer-Friedrich, B., 2019. Antimonite complexation with thiol and carboxyl/phenol groups of peat organic matter. Environ. Sci. Technol. 53 (9), 5005–5015.

Biver, M., Krachler, M., Shotyk, W., 2011. The desorption of antimony(V) from sediments, hydrous oxides, and clay minerals by carbonate, phosphate, sulfate, nitrate, and chloride. J. Environ. Qual. 40 (4), 1143–1152.

Burton, E.D., Hockmann, K., Karimian, N., Johnston, S.G., 2019. Antimony mobility in reducing environments: the effect of microbial iron(III)-reduction and associated secondary mineralization. Geochim. Cosmochim. Acta 245, 278–289.

Burton, E.D., Hockmann, K., Karimian, N., 2020. Antimony sorption to goethite: effects of Fe(II)-catalyzed recrystallization. ACS Earth Space Chem. 4 (3), 476–487.

Cai, Y.B., Mi, Y.T., Zhang, H., 2016. Kinetic modeling of antimony(III) oxidation and sorption in soils. J. Hazard. Mater. 316, 102–109.

Chen, N., Fu, Q., Wu, T., Cui, P., Fang, G., Liu, C., Chen, C., Liu, G., Wang, W., Wang, D., Wang, P., Zhou, D., 2021. Active iron phases regulate the abiotic transformation of organic carbon during redox fluctuation cycles of paddy soil. Environ. Sci. Technol. 55 (20), 14281–14293.

Cui, Y., Weng, L., 2013. Arsenate and phosphate adsorption in relation to oxides composition in soils: LCD modeling. Environ. Sci. Technol. 47 (13), 7269–7276.

Davis, J.A., Coston, J.A., Kent, D.B., Fuller, C.C., 1998. Application of the surface complexation concept to complex mineral assemblages. Environ. Sci. Technol. 32 (19), 2820–2828.

Doherty, S., Tighe, M.K., Milan, L.A., Johannessen, B., Mitchell, V., Hamilton, J., Johnston, S.G., Wilson, S.C., 2021. Long-range spatial variability in sediment associations and solid-phase speciation of antimony and arsenic in a mining-impacted river system. Appl. Geochem. 135, 105112.

Dou, X., Mohan, D., Zhao, X., Pittman Jr, C.U., 2015. Antimonate removal from water using hierarchical macro-/mesoporous amorphous alumina. Chem. Eng. J. 264, 617–624.

Dousova, B., Buzek, F., Herzogova, L., Machovic, V., Lhotka, M., 2015. Effect of organic matter on arsenic(V) and antimony(V) adsorption in soils. Eur. J. Soil Sci. 66 (1), 74–82.

Fan, J.X., Wang, Y.J., Cui, X.D., Zhou, D.M., 2013. Sorption isotherms and kinetics of Sb (V) on several Chinese soils with different physicochemical properties. J. Soils Sed. 13 (2), 344–353.

Fox, P.M., Davis, J.A., Luther III, G.W., 2009. The kinetics of iodide oxidation by the manganese oxide mineral birnessite. Geochim. Cosmochim. Acta 73 (10), 2850–2861.

Gallard, H., Allard, S., Nicolau, R., von Gunten, U., Croue, J.P., 2009. Formation of iodinated organic compounds by oxidation of iodide-containing waters with manganese dioxide. Environ. Sci. Technol. 43 (18), 7003–7009.

Ginder-Vogel, M., Landrot, G., Fischel, J.S., Sparks, D.L., 2009. Quantification of rapid environmental redox processes with quick-scanning X-ray absorption spectroscopy (Q-XAS). Proc. Natl. Acad. Sci. U. S. A. 106 (38), 16124–16128.

Guo, X., Wu, Z., He, M., Meng, X., Jin, X., Qiu, N., Zhang, J., 2014. Adsorption of antimony onto iron oxyhydroxides: adsorption behavior and surface structure. J. Hazard. Mater. 276 (9), 339–345.

He, M., Wang, N., Long, X., Zhang, C., Ma, C., Zhong, Q., Wang, A., Wang, Y., Pervaiz, A., Shan, J., 2018. Antimony speciation in the environment: recent advances in understanding the biogeochemical processes and ecological effects. J. Environ. Sci. 75, 14–39.

Hockmann, K., Karimian, N., Schlagenhauff, S., Planer-Friedrich, B., Burton, E.D., 2021. Impact of antimony(V) on iron(II)-catalyzed ferrihydrite transformation pathways: a novel mineral switch for feroxyhyte formation. Environ. Sci. Technol. 55 (8), 4954–4963.

Ianni, J.C., 2018. Kintecus. Windows Version 6.50, www.kintecus.com.

Ilgen, A.G., Trainor, T.P., 2011. Sb (III) and Sb (V) sorption onto Al-rich phases: hydrous Al oxide and the clay minerals kaolinite KGa-1b and oxidized and reduced nontronite NAu-1. Environ. Sci. Technol. 46 (2), 843–851.

Kleber, M., Eusterhues, K., Keiluweit, M., Mikutta, C., Mikutta, R., Nico, P.S., 2015. Mineral-organic associations: formation, properties, and relevance in soil environments. In: D.L. Sparks (Ed.), Adv. Agron. 130, 1-140.

Kong, L.H., He, M.C., 2016. Mechanisms of Sb (III) photooxidation by the excitation of organic Fe(III) complexes. Environ. Sci. Technol. 50 (13), 6974–6982.

Kong, L.H., Hu, X.Y., He, M.C., 2015. Mechanisms of Sb(III) oxidation by pyrite-induced hydroxyl radicals and hydrogen peroxide. Environ. Sci. Technol. 49 (6), 3499–3505.

Lehmann, J., Kleber, M., 2015. The contentious nature of soil organic matter. Nature 528 (7580), 60–68.

Leuz, A.K., 2006. Redox reactions of antimony in the aquatic and terrestrial environment. Switzerland, ETH Zurich.

Leuz, A.K., Johnson, C.A.R., 2005. Oxidation of Sb(III) to Sb(V) by O_2 and H_2O_2 in aqueous solutions. Geochim. Cosmochim. Acta 69 (5), 1165–1172.

Leuz, A.K., Moench, H., Johnson, C.A., 2006. Sorption of Sb(III) and Sb(V) to goethite: Influence on Sb(III) oxidation and mobilization. Environ. Sci. Technol. 40 (23), 7277–7282.

Li, J., Hou, H., Hosomi, M., 2018. Sorption-desorption of Sb(III) in different soils: Kinetics and effects of the selective removal of hydroxides, organic matter, and humic substances. Chemosphere 204, 371–377.

Liu, Z.P., Shao, M.A., Wang, Y.Q., 2013. Spatial patterns of soil total nitrogen and soil total phosphorus across the entire Loess Plateau region of China. Geoderma 197, 67–78.

Lu, R., 2000. Soil and Agro-chemistry Analysis. China Agriculture Science and Technique Press, Beijing, China (in Chinese).

Manning, B.A., Suarez, D.L., 2000. Modeling arsenic(III) adsorption and heterogeneous oxidation kinetics in soils. Soil Sci. Soc. Am. J. 64 (1), 128–137.

Martinez-Llado, X., Valderrama, C., Rovira, M., Marti, V., Gimenez, J., de Pablo, J., 2011. Sorption and mobility of Sb(V) in calcareous soils of Catalonia (NE Spain): Batch and column experiments. Geoderma 160 (3–4), 468–476.

Mitsunobu, S., Takahashi, Y., Terada, Y., 2010. μ-XANES evidence for the reduction of Sb (V) to Sb(III) in soil from Sb mine tailing. Environ. Sci. Technol. 44 (4), 1281–1287.

Mitsunobu, S., Muramatsu, C., Watanabe, K., Sakata, M., 2013. Behavior of antimony(V) during the transformation of ferrihydrite and its environmental implications. Environ. Sci. Technol. 47 (17), 9660–9667.

Nakamaru, Y., Tagami, K., Uchida, S., 2006. Antimony mobility in Japanese agricultural soils and the factors affecting antimony sorption behavior. Environ. Pollut. 141 (2), 321–326.

Power, L.E., Arai, Y., Sparks, D.L., 2005. Zinc adsorption effects on arsenite oxidation kinetics at the birnessite-water interface. Environ. Sci. Technol. 39 (1), 181–187.

Pullin, M.J., Cabaniss, S.E., 2003. The effects of pH, ionic strength, and iron-fulvic acid interactions on the kinetics of nonphotochemical iron transformations. I. Iron(II) oxidation and iron(III) colloid formation. Geochim. Cosmochim. Acta 67 (21), 4067–4077.

Rahman, M.S., Clark, M.W., Yee, L.H., 2019. Arsenic(V) sorption kinetics in long-term arsenic pesticide contaminated soils. Appl. Geochem. 111, 104444.

Scheinost, A.C., Rossberg, A., Vantelon, D., Xifra, I., Kretzschmar, R., Leuz, A.-K., Funke, H., Johnson, C.A., 2006. Quantitative antimony speciation in shooting-range soils by EXAFS spectroscopy. Geochim. Cosmochim. Acta 70 (13), 3299–3312.

Shi, Z.Q., Peng, S.M., Wang, P., Sun, Q., Wang, Y.J., Lu, G., Dang, Z., 2018. Modeling coupled kinetics of antimony adsorption/desorption and oxidation on manganese oxides. Environ. Sci. Proc. Impacts 20 (12), 1691–1696.
Shuman, L.M., 1982. Separating soil iron-oxide and manganese-oxide fractions for micro-element analysis. Soil Sci. Soc. Am. J. 46 (5), 1099–1102.
Sun, Q., Liu, C., Alves, M.E., Ata-Ul-Karim, S.T., Zhou, D.M., He, J.Z., Cui, P.X., Wang, Y. J., 2018. The oxidation and sorption mechanism of Sb on δ-MnO_2. Chem. Eng. J. 342, 429–437.
Sun, Q., Cui, P.X., Liu, C., Peng, S.M., Alves, M.E., Zhou, D.M., Shi, Z.Q., Wang, Y.J., 2019. Antimony oxidation and sorption behavior on birnessites with different properties (δ-MnO_2 and triclinic birnessite). Environ. Pollut. 246, 990–998.
Sun, Q., Liu, C., Fan, T.T., Cheng, H., Cui, P.X., Gu, X.Y., Chen, L.N., Ata-Ul-Karim, S.T., Zhou, D.M., Wang, Y.J., 2023. A molecular level understanding of antimony immobilization mechanism on goethite by the combination of X-ray absorption spectroscopy and density functional theory calculations. Sci. Total Environ. 865, 161294.
Tighe, M., Lockwood, P., Wilson, S., 2005. Adsorption of antimony(V) by floodplain soils, amorphous iron(III) hydroxide and humic acid. J. Environ. Monit. 7 (12), 1177–1185.
Tombacz, E., Libor, Z., Illes, E., Majzik, A., Klumpp, E., 2004. The role of reactive surface sites and complexation by humic acids in the interaction of clay mineral and iron oxide particles. Org. Geochem. 35 (3), 257–267.
Verbeeck, M., Moens, C., Gustafsson, J.P., 2021. Mechanisms of antimony ageing in soils: An XAS study. Appl. Geochem. 128, 104936.
Villalobos, M., Escobar-Quiroz, I.N., Salazar-Camacho, C., 2014. The influence of particle size and structure on the sorption and oxidation behavior of birnessite: I. Adsorption of As(V) and oxidation of As(III). Geochim. Cosmochim. Acta 125, 564–581.
Vithanage, M., Rajapaksha, A.U., Dou, X., Bolan, N.S., Yang, J.E., Ok, Y.S., 2013. Surface complexation modeling and spectroscopic evidence of antimony adsorption on iron-oxide-rich red earth soils. J. Colloid Interface Sci. 406, 217–224.
Wang, Y.J., Fan, T.T., Cui, P.X., Sun, Q., Zhou, D.M., Li, C.B., Wang, G.Q., Lin, Y.S., Zhang, S.T., Yang, X.P., Zhao, F.J., Friedman, S.P., 2020. Binding and adsorption energy of Cd in soils and its environmental implication for Cd bioavailability. Soil Sci. Soc. Am. J. 84 (2), 472–482.
Wang, X., Yang, Y., Tao, L., He, M., 2021. Antimonite oxidation and adsorption onto two tunnel-structured manganese oxides: Implications for antimony mobility. Chem. Geol. 579, 120336.
Wilson, S.C., Lockwood, P.V., Ashley, P.M., Tighe, M., 2010. The chemistry and behaviour of antimony in the soil environment with comparisons to arsenic: a critical review. Environ. Pollut. 158 (5), 1169–1181.
Wu, T.L., Qin, W.X., Alves, M.E., Fang, G.D., Sun, Q., Cui, P.X., Liu, C., Zhou, D.M., Wang, Y.J., 2019a. Mechanisms of Sb(III) oxidation mediated by low molecular weight phenolic acids. Chem. Eng. J. 356, 190–198.
Wu, T.L., Sun, Q., Fang, G.D., Cui, P.X., Liu, C., Alves, M.E., Qin, W.X., Zhou, D.M., Shi, Z. Q., Wang, Y.J., 2019b. Unraveling the effects of gallic acid on Sb (III) adsorption and oxidation on goethite. Chem. Eng. J. 369, 414–421.
Xia, B., Yang, Y., Li, F., Liu, T., 2022. Kinetics of antimony biogeochemical processes under pre-definite anaerobic and aerobic conditions in a paddy soil. J. Environ. Sci. 113, 269–280.
Ying, S.C., Kocar, B.D., Fendorf, S., 2012. Oxidation and competitive retention of arsenic between iron- and manganese oxides. Geochim. Cosmochim. Acta 96, 294–303.
Zhang, Y., O'Loughlin, E.J., Kwon, M.J., 2022. Antimony redox processes in the environment: A critical review of associated oxidants and reductants. J. Hazard. Mater. 431, 128607-128607.
Zhang, C., He, M., Ouyang, W., Lin, C., Liu, X., 2020. Influence of Fe(II) on Sb(III) oxidation and adsorption by MnO_2 under acidic conditions. Sci. Total Environ. 724, 138209.
Zhang, H., Li, L., Zhou, S., 2014. Kinetic modeling of antimony(V) adsorption-desorption and transport in soils. Chemosphere 111, 434–440.